

Modulation of the Electron Redistribution in Mixed Valence Cytochrome *c* Oxidase by Protein Conformational Changes*

Received for publication, September 29, 2003, and in revised form, November 12, 2003
Published, JBC Papers in Press, December 5, 2003, DOI 10.1074/jbc.M310729200

Hong Ji, Syun-Ru Yeh, and Denis L. Rousseau‡

From the Department of Physiology and Biophysics, Albert Einstein College of Medicine of Yeshiva University, Bronx, New York 10461

The redistribution of two electrons in the four redox centers of cytochrome *c* oxidase following photodissociation of CO from the CO-bound mixed valence species has been examined by resonance Raman spectroscopy. To account for both the kinetic data, obtained from 5 μ s to 2 ms, and the equilibrium results, a model is proposed in which the electron redistribution is modulated by a protein conformation transition from a nascent P₁ state to a relaxed P₂ state in a time window longer than 2 ms. In this model, all six possible two-electron reduced species are considered. The high population of species with a one-electron reduced binuclear center, in which the spectrum of heme a₃ is perturbed by the redox state of Cu_B, accounts for the significant residuals in the fitting of the kinetic data with four standard spectra derived from redox species with either zero or two electrons in the binuclear center. Under equilibrium conditions, the conformational change to the P₂ state destabilizes the redox states with only one electron in the binuclear center with respect to those with either zero or two electrons. As a result, the redox equilibrium is perturbed, and the electrons are redistributed. A simulation based on the new kinetics scheme, in which the electron redistribution is modulated by the protein conformation, gives reasonable agreement with both the equilibrium and the kinetic data, demonstrating the validity of this model.

Cytochrome *c* oxidase, (CcO¹; ferrocytochrome *c*: O₂ oxidoreductase, EC 1.9.3.1), the terminal enzyme in the electron transport chain, catalyzes the four-electron reduction of oxygen to water. Associated with the oxygen reduction chemistry, four protons are pumped across the mitochondrial inner membrane, contributing to the proton motive force required for ATP synthesis. The enzyme contains four redox centers: two hemes and two copper centers termed heme a, heme a₃, Cu_A, and Cu_B, respectively. Under physiological conditions, the electron donor, cytochrome *c*, donates electrons to Cu_A, which is located near the cytochrome *c* binding site. The electrons in Cu_A are subsequently transferred to heme a and then to the binuclear center consisting of heme a₃ and Cu_B, where oxygen reduction occurs (1–4). It requires four electrons for one molecule of

oxygen to be reduced to two molecules of water. It is very important to understand the electron transfer events to fully determine the molecular mechanism underlying this important enzyme. However, it is a non-trivial task to study the forward electron transfer reactions because they are tightly coupled with the oxygen reduction chemistry. On the other hand, flash photolysis of the so-called mixed valence CO-bound derivative (MVCO) has been extensively used to study the reverse electron transfer reactions in CcO (5–8).

The MVCO species is a two-electron reduced derivative in which heme a₃ and Cu_B are reduced, whereas the other two redox centers, heme a and Cu_A, remain oxidized. The reduced state of the binuclear center in MVCO is stabilized by a CO molecule bound to the iron atom of heme a₃. Photolysis of CO lowers the redox potential of the binuclear center, reversing about electron redistribution with electron flow in the reverse direction from the binuclear center to heme a and Cu_A (9–11). With a known equilibrium constant, the forward electron transfer rate can be extracted from the observed rate constant that is the sum of the forward and reverse rate constants.

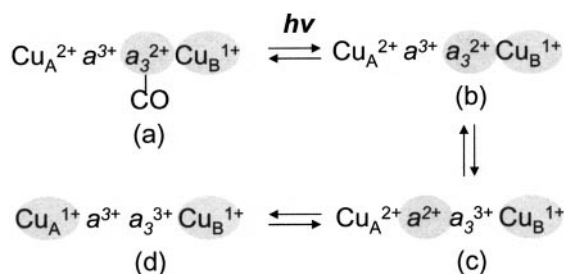
Scheme 1 illustrates a generally accepted electron transfer mechanism associated with photolysis of MVCO (species a). Immediately following photolysis, a ligand-free species, b, is formed. It is followed by an electron transfer reaction from heme a₃ to heme a that leads to species c. The subsequent electron transfer from heme a to Cu_A produces species d. Each step in the electron transfer chain described in Scheme 1 is reversible. In addition, it is believed that one electron always resides on Cu_B because it is proposed to have a midpoint potential that is much higher than those of the two hemes (6, 8).

Two fast kinetic phases have been reported for the electron transfer reactions in bovine CcO. The first phase is assigned to the electron transfer from heme a₃ to heme a, which occurs at a rate of $\sim 3 \times 10^5$ s⁻¹ (8, 12, 13). It is followed by electron transfer from heme a to Cu_A at about 2×10^4 s⁻¹. Similar studies have been carried out on other members of the terminal oxidase super family, including those from the bacterium *Rhodobacter sphaeroides* and cytochrome bo₃ from *Escherichia coli* (12, 14, 15), and the electron transfer events in these enzymes were detected on similar time scales. Recently, the rates and the extent of the electron transfer were questioned by Verkhovsky *et al.* (16), who reported that an electron transfer event between the two hemes occurs on a time scale much faster than 100 ns, the limit of their instrumental resolution, and accounted for about 50% amplitude of the total amount of electron transfer from heme a₃ to heme a. However, after reinvestigation of this reaction, Namslauer *et al.* (17) concluded that no evidence was found for the presence of this early phase. Instead, they reported that the microscopic forward and reverse rate constants for the electron-transfer reactions from heme a to heme a₃ are not faster than $\sim 2 \times 10^5$ and $\sim 1 \times 10^5$ s⁻¹, respectively.

* This work was supported by the National Institute of Health Research Grants HL65465 (to S.-R. Y.) and GM54806 (to D. L. R.). The costs of publication of this article were defrayed in part by the payment of page charges. This article must therefore be hereby marked "advertisement" in accordance with 18 U.S.C. Section 1734 solely to indicate this fact.

‡ To whom correspondence should be addressed. Tel.: 718-430-4264; Fax: 718-430-8808; E-mail: rousseau@aecom.yu.edu.

¹ The abbreviations used are: CcO, cytochrome *c* oxidase; MVCO, mixed valence CO-bound derivative; W, watts.



SCHEME 1

In addition to the fast phases, millisecond time scale changes were also observed that were ascribed to the structural rearrangement associated with the electron redistribution and/or CO recombination (6, 7). Based on optical absorption spectroscopy, Einarsdottir and co-workers (5, 6) pointed out that in addition to the four species included in Scheme 1, other intermediates have to be considered to account for the changes observed in the optical spectra.

To clarify the electron transfer reaction mechanism, we used resonance Raman spectroscopy to reinvestigate the intramolecular electron transfer events following photolysis of MVCO. Resonance Raman spectroscopy is a sensitive probe for detecting electron density and structural dynamics of heme prosthetic groups in heme proteins. It has been proved to be a powerful technique for characterizing the structural properties of reaction intermediates and associated kinetics in various heme proteins (18). With resonance Raman spectroscopy, we demonstrate that the electron transfer reaction following photolysis of MVCO is associated with a conformational transition that regulates the electron redistribution in the four redox centers of CcO.

MATERIALS AND METHODS

CcO was purified from beef hearts by the method described by Yoshikawa *et al.* (19). The enzyme was dissolved in 0.01 M sodium phosphate buffer at pH 7.4 with 0.1% *n*-decyl- β -maltoside as the detergent. The protein solution was stored in liquid nitrogen until further use. The enzyme concentration was determined by the optical absorption intensity difference of the fully reduced form at 604 nm minus that of fully oxidized form at 630 nm with 23.3 $\text{mM}^{-1} \text{cm}^{-1}$ as the extinction coefficient difference.

In the equilibrium experiments, the CcO stock solution was diluted to 40 μM with 0.1 M, pH 7.4, sodium phosphate buffer including 0.1% *n*-dodecyl- β -maltoside. The MVCO was prepared by incubating the purified resting enzyme under a CO atmosphere in the absence of O_2 for about 6 h in a sealed Raman cell. The formation of MVCO was confirmed by the optical absorption spectrum with characteristic bands at 428 and 590 nm. Prior to the resonance Raman measurements, the atmosphere inside the Raman cell was purged with high purity nitrogen to lower the CO concentration to minimize CO recombination following photolysis. The output at 413.1 nm from a krypton ion laser with a power of 8 mW was applied to simultaneously photodissociate the CO and to probe the resonance Raman spectrum. The Raman cell was rotated at ~ 6000 rpm to avoid photoreduction and/or photodamage. The Raman apparatus has been described elsewhere (18). The spectral acquisition time for a typical spectrum was 30 s.

For the microsecond kinetic measurements, a continuous-flow technique, described previously, was used to study the microsecond kinetics of the electron transfer reaction following photodissociation of MVCO (20). This is an adaptation of the flow-flash-probe method originally pioneered by Gibson and Greenwood (21). MVCO (100 μM) was prepared in a homemade glassware apparatus consisting of a round bottom flask with an optical absorption cuvette attached to it. The round bottom flask provides a large surface area to ensure that the resting enzyme is fully exposed to the CO atmosphere, and the attached cuvette enables the confirmation of the formation of MVCO *in situ* by optical absorption measurements. Once MVCO was produced, it was transferred to glass syringes in a nitrogen-filled glove box to prevent oxygen contamination. During the measurements, the MVCO sample in the syringes was driven to an oxygen-free observation cell with a mechan-

ical syringe pump at a constant speed. The dimensions of the observation cell are $250 \times 250 \mu\text{m}$. One 413.1-nm laser beam (the pump beam) with a power of ~ 270 mW was used to photolyze the sample. The other 413.1-nm laser beam (the probe beam, ~ 120 mW), which was spatially separated from the pump beam, was used to probe the resonance Raman spectra. The reaction time was selected by adjusting the flow rate and the distance between the pump and the probe beams. The earliest observable time point was $\sim 5 \mu\text{s}$ with the fastest linear flow rate of 7 m/s and with the pump beam overlapping with the probe beam. The pump beam was sharply focused with a cylindrical lens, resulting in a 35- μm -thin slab on the sample to ensure that the sample to be probed is fully photolyzed. The typical spectral acquisition time was 45 s.

The spectra used for the calculation of the standard spectra for spectral deconvolution were obtained with 413.1-nm laser excitation. The intensity was normalized with an internal standard, potassium sulfate (0.5 M), and the deconvolution program was written with a commercial software package, Mathcad.

RESULTS

Generation of the Standard Spectra—Based on Scheme 1, at least four species are expected during the photolysis experiments. The spectrum of species a can be directly obtained from MVCO (Fig. 1, *spectrum A*). On the other hand, species b and c are metastable species that cannot be measured directly. We sought to calculate their spectra by a linear combination of the spectra of various redox species that can be easily obtained under equilibrium conditions. Fig. 1, *spectrum B*, is derived by adding the spectrum of the fully reduced form ($\text{Cu}_A^{1+} a^{2+} a_3^{2+} \text{Cu}_B^{1+}$) to that of the MVCO form ($\text{Cu}_A^{2+} a^{3+} a_3^{2+} \text{CO-Cu}_B^{1+}$) and subtracting out that of the CO-bound fully reduced form ($\text{Cu}_A^{1+} a^{2+} a_3^{2+} \text{CO-Cu}_B^{1+}$). The result of this calculation is $\text{Cu}_A^{2+} a^{3+} a_3^{2+} \text{Cu}_B^{1+}$, exactly the same as species b shown in Scheme 1. Likewise, spectrum C is derived by adding the spectrum of the CO-bound fully reduced form to that of the fully oxidized form and subtracting out that of MVCO. The result of this calculation is $\text{Cu}_A^{1+} a^{2+} a_3^{3+} \text{Cu}_B^{2+}$. It is important to note that the redox states of heme a and a_3 in this calculated spectrum are the same as that of species c, but the copper centers adopt different redox states. However, with a 413.1-nm excitation, which is nearly in resonance with the Soret absorption of this enzyme, only the vibrational modes of the hemes are enhanced; therefore, the calculated spectrum should represent that of species c if the redox states of the copper centers do not perturb the heme spectra (this assumption came into question as will be discussed later). Likewise, spectrum D from the fully oxidized enzyme with $\text{Cu}_A^{2+} a^{3+} a_3^{3+} \text{Cu}_B^{2+}$ redox centers is used to mimic species d, although the redox states of the copper centers are not identical. It is important to point out that all the initial spectra used to generate the four standard spectra have either zero or two electrons in the binuclear center.

Equilibrium Measurements—The output at 413.1 nm from a krypton ion laser was employed to photodissociate CO from MVCO and to probe the extent of the subsequent electron transfer from heme a_3 to heme a. To avoid photoreduction, the laser power was kept low, and the MVCO enzyme was placed in a rapidly rotating cell. Under these conditions, a photostationary state was reached at ~ 15 min following the initiation of the photolysis. Fig. 2 shows the resonance Raman spectra of a series of MVCO samples measured at various laser irradiation times. Progressive spectral changes in several of the modes are evident: 1) the decrease in the intensity of the electron density marker line (ν_4) of the CO bound heme a_3^{2+} at 1368 cm^{-1} ; 2) the increase in intensity of the high spin marker line (ν_2) at 1570 cm^{-1} of the ligand-free heme a_3^{3+} ; and 3) the decrease in the intensity of the reduced heme a_3 formyl line at 1667 cm^{-1} . These changes reflect the photodissociation of CO from heme a_3 and its conversion to a ferric heme due to the subsequent electron transfer to heme a. The electron transfer from heme a_3

FIG. 1. Basis spectra of the four possible redox states used for the spectral deconvolution. *A*, mixed valence CO-bound form of the enzyme (MVCO). *B*, calculated spectrum obtained by adding the spectrum of the fully reduced form to that of the MVCO form and subtracting out that of the fully reduced CO-bound form. *C*, calculated spectrum obtained by adding the spectrum of the CO-bound reduced form and subtracting out that of the MVCO form. *D*, fully oxidized form. The redox and ligation states of the hemes are indicated in each spectrum. See details under "Results."

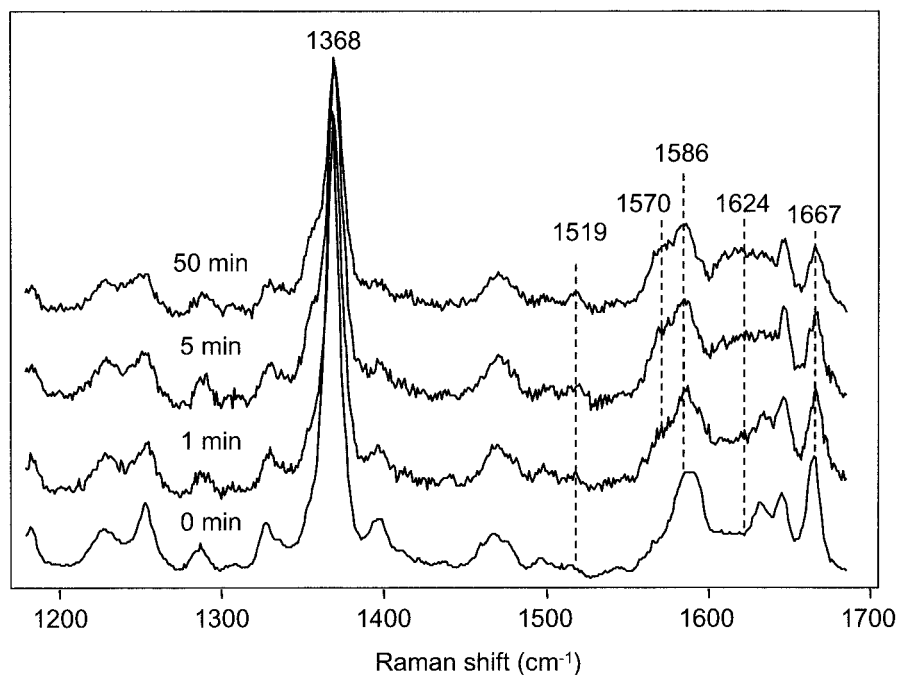
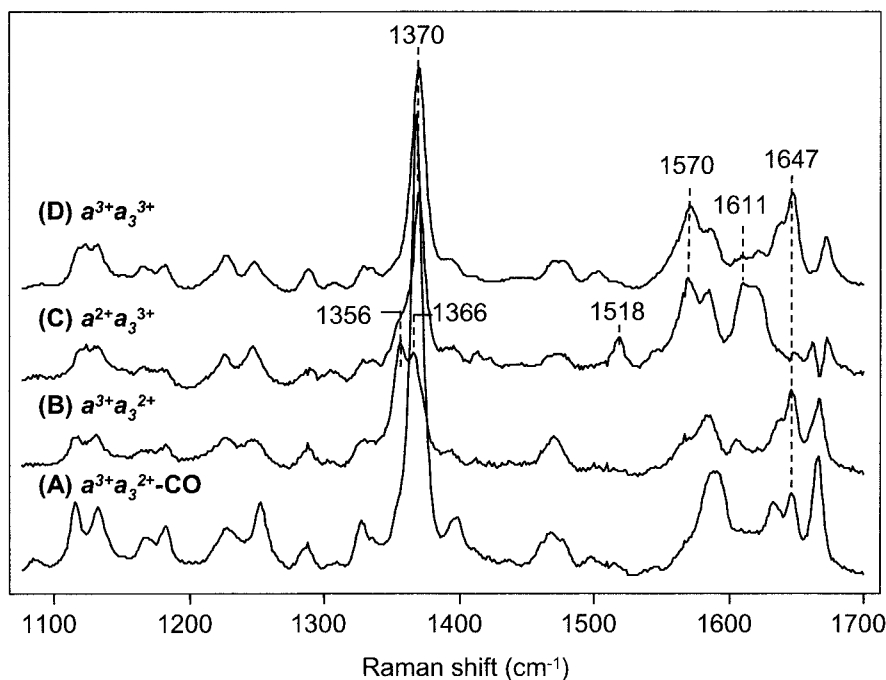


FIG. 2. Resonance Raman spectra under photostationary state conditions obtained by photolyzing the CO-bound mixed valence enzyme with a 413.1-nm laser beam. The duration of the light exposure is indicated in each spectrum. The spectrum labeled 0 min is that of the CO-bound mixed valence enzyme obtained at very low laser power (0.7 mW to prevent photodissociation) and long acquisition time.

to heme *a* is also evident from the increase in the intensity of the marker lines for the reduced state of heme *a* at 1519 and 1624 cm^{-1} .

To obtain quantitative information, each of the experimental spectra was deconvoluted into the four basis spectra presented in Fig. 1. All the experimental spectra can be fully accounted for by the basis spectra as demonstrated by a typical deconvolution result shown in Fig. 3. The negligible residuals from the fitting displayed at the bottom of the figure demonstrate that there are no additional spectral intermediates present during the reaction other than the four spectra shown in Fig. 1. The population of each spectral component was plotted as a function of the exposure time in Fig. 4. It is evident that the population of the photolyzed species increases as the exposure time increases, and the contribution from spectrum *D* is negli-

gible during the full course of photolysis. Furthermore, under the photostationary state, 30% of *B* and 40% of *C* were observed. The rest of the molecules are in the CO-bound mixed valence state due to limited photolysis resulting from the low laser power and to CO rebinding. Under the conditions applied here, photolyzed CO from MVCO rebinds to heme a_3 on the 10–100-ms time scale (22). With the speed of the rotating cell set at ~ 6000 rpm, a very low degree of photolysis and a significant amount of CO rebinding is expected under the photostationary conditions. Based on the results shown in Fig. 4, in the photolyzed fraction of the enzyme, $\sim 60\%$ of the electron density originally stabilized in heme a_3 is transferred to heme *a*. This conclusion is consistent with the results observed by others; for example, see Verkhovsky *et al.* (16).

Microsecond Time-resolved Measurements—A flow-flash-

FIG. 3. A typical deconvolution of the data shown in Fig. 2 with the basis spectra shown in Fig. 1. This spectrum was obtained with a 35-min-duration laser exposure. The residuals at the bottom are the difference between the raw data and the fitted spectrum.

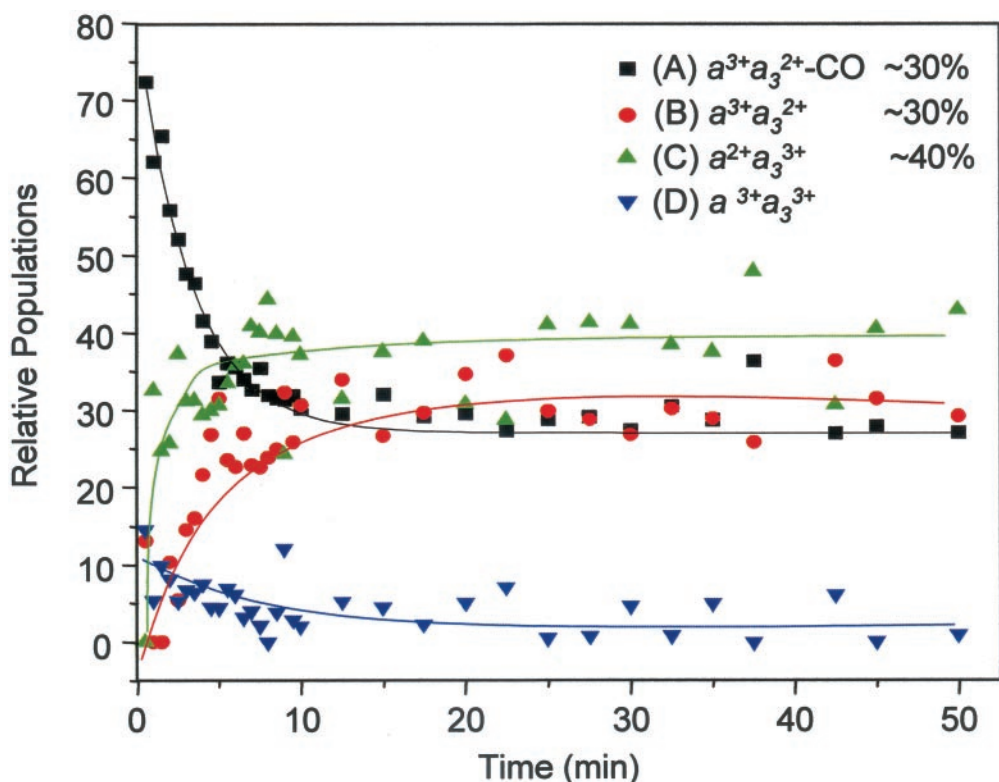
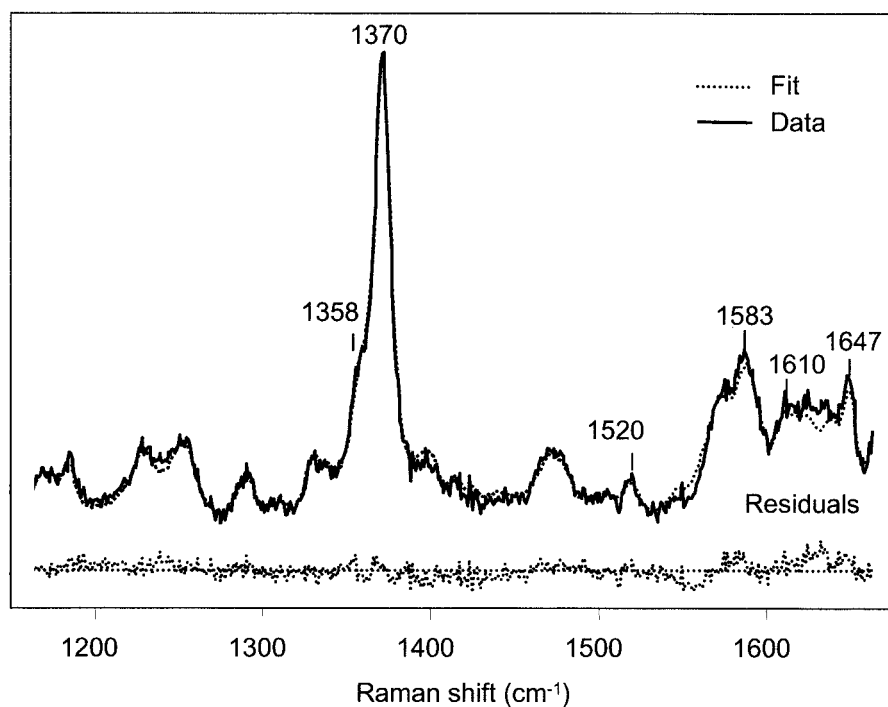


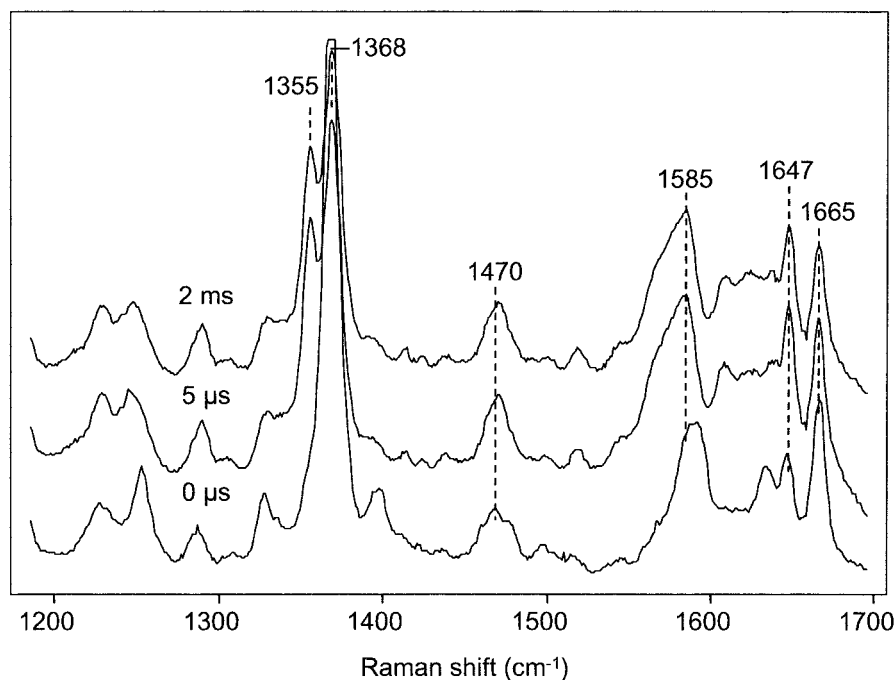
FIG. 4. Time-dependent population changes of each of the spectral species as a function of the laser exposure obtained by deconvoluting the photostationary state data into the basis spectra. The populations of each species under the photostationary state conditions are listed in the figure.

probe method, as described under "Materials and Methods," was adapted to resolve the kinetics of the electron transfer reaction. The time-resolved resonance Raman spectra following photolysis are shown in Fig. 5. The spectrum labeled 0 μ s represents the spectrum of the MVCO species that is obtained without photolysis. The spectrum labeled 5 μ s, the earliest detectable time point, is obtained by overlapping the pump and the probe beams. Significant changes are observed between the

MVCO and the 5- μ s spectrum, confirming that CO is photolyzed from MVCO. However, the spectrum at 2 ms (the longest time point that can be measured with the current setup) is virtually the same as that at 5 μ s, indicating that no further electron transfer takes place between 5 μ s and 2 ms. Similar observations were made by using independent preparations of the enzyme confirming the reliability of these results.

The 5- μ s spectrum is deconvoluted with the four standard

FIG. 5. Time-resolved resonance Raman spectra following photodissociation of the mixed valence CO-bound derivative by the flow-flash-probe method. The reaction times are as indicated. The spectrum labeled $0 \mu\text{s}$ was obtained prior to the photodissociation.



spectra shown in Fig. 1. The contributions from A–D are estimated to be 0, 60, 27, and 13%, respectively. However, in contrast to the equilibrium data (Fig. 3), the residuals from the fitting are significant, as shown in Fig. 6, *bottom*. Due to the unsatisfactory fit, efforts were also made to deconvolute the experimental spectrum with the fully reduced and fully reduced CO-bound spectra in addition to spectra A–D. Although the spectra include all the possible combinations of the heme redox states, $(a^{2+}a_3^{2+})$, $(a^{3+}a_3^{2+})$, $(a^{2+}a_3^{3+})$, and $(a^{3+}a_3^{3+})$, we were unable to obtain good fits. Therefore, it is concluded that under the transient conditions applied here in the kinetic experiments, either the four spectra are not a valid set of basis spectra, or the four spectra are a valid set of basis spectra, there is at least one additional intermediate that has not been accounted for.

DISCUSSION

The spectral deconvolution method applied here for the quantitative analysis of the intermolecular electron transfer reactions of CcO is carried out based on the assumption that all of the spectral features in the resonance Raman spectra originate from the heme groups, that the calculated basis spectra are representative of the authentic intermediates, and that no additional intermediates are present. The excellent fit of the equilibrium data with the four standard spectra (Fig. 3) confirms the validity of these assumptions with this method. However, the fit does not address the validity of Scheme 1 because the redox states of Cu_B in species c and d (Scheme 1) are different from those associated with spectra C and D (Fig. 1), as will be discussed later. On the other hand, the calculated spectrum B for the species b is the same as that of the 10-ns photoproduct of MVCO reported by Proshlyakov *et al.* (23), confirming the authenticity of this spectrum for species b. In addition, the consistency of these two spectra indicates that at 10 ns, the CO has already been cleaved from heme a_3 and that the initial electron transfer from heme a_3 to heme a takes longer than 10 ns. Based on this conclusion, we exclude the possibility for the existence of the ultrafast electron tunneling phase with a rate of $\geq 10^8 \text{ s}^{-1}$ reported by Verkhovsky *et al.* (16).

The failure to obtain a good fit of the kinetic data indicates

that there are some new intermediates that cannot be accounted for by the standard spectra shown in Fig. 1. A spectral contribution from non-heme species is excluded because it is well established that in the resonance Raman spectra with Soret excitation, only the heme vibrational modes are detectable due to their strong enhancement. To account for these new intermediates, we propose a new kinetic model in which all six possible oxidation states of the two-electron reduced CcO are considered, as illustrated in Scheme 2. We also postulate that the resonance Raman spectrum of heme a_3 in the redox states c, c', d, and d', which consist of a one-electron reduced binuclear center, is perturbed by the redox state of Cu_B . As a consequence, the spectra of the intermediates c, c', d, and d' cannot be accounted by the standard spectra derived from the equilibrium species with either zero or two electrons in the binuclear center. An influence on the heme a_3 spectrum by Cu_B is not unexpected because Cu_B is only 4.7 Å away from heme a_3 (24). Perturbations of the optical absorption spectra, likely related to our observations, obtained following photolysis MVCO were reported by others on the millisecond time scale and have been attributed to a conformational change (6).

In the model proposed here, species b is produced within 10 ns following photodissociation of CO from MVCO. The electron in heme a_3 is subsequently transferred to heme a and then to Cu_A , leading to species c and d, respectively. We propose that the single electron in the binuclear center in species c and d is delocalized on heme a_3 and Cu_B as reflected by the equilibrium between c and c' and that between d and d'. Electron delocalization in heme a_3 and Cu_B in the binuclear center is not unprecedented. It has been reported in the past that the electrons can reside on heme a, heme a_3 , or the Cu_B site when CcO is not fully reduced (25–30). It is postulated that the electron in heme a_3 in species d' can further transfer to heme a, leading to species e. The significant population of c, c', d, and d' during the reaction accounts for the unsatisfactory fit of the data with the equilibrium spectra because the resonance Raman spectrum of heme a_3 in these redox species is perturbed by the redox state of Cu_B .

To account for the equilibrium photostationary data, we propose that following photodissociation of the mixed valence spe-

equilibrium binding to Cu_B followed by a unimolecular transfer to heme a_3 (22). Under our concentration conditions, the observed rate of CO rebinding to heme a_3 is expected to be $\sim 10 \text{ s}^{-1}$. This is consistent with our observation of the absence of any MVCO species in the kinetic measurements in contrast to its presence in the photostationary experiments.

The first set of rate constants, k_{2f} and k_{2r} , associated with the electron transfer from heme a_3 to heme a are estimated to be $\sim 1 \times 10^5$ and $\sim 2 \times 10^5 \text{ s}^{-1}$, respectively, based on recent studies by Namslauer *et al.* (17). The second set of rate constants, k_{3f} and k_{3r} , associated with the electron transfer from heme a to Cu_A , are assigned values of 1×10^4 and $7 \times 10^3 \text{ s}^{-1}$, respectively, based on the photolysis studies carried out in a three-electron-reduced CO-bound form of the enzyme, in which heme a and Cu_A were partially reduced and in a redox equilibrium (32). The rate constants, k_{4f} and k_{4r} , associated with the electron transfer from Cu_B to heme a_3 have not been reported. We assume that the redox equilibrium between c and c' and that between d and d' are much faster than k_{3f} and k_{3r} . For a rough approximation that satisfies the pre-equilibrium assumption, k_{4f} and k_{4r} are assumed to be 50 times faster than k_{3f} . It should be noted that the selection of these rate constants does not affect the qualitative results of the simulations, provided they satisfy the pre-equilibrium conditions. The rate constants, k_{5f} and k_{5r} , associated with the conversation from d' to e are approximated to be the same as k_{2f} ($1 \times 10^5 \text{ s}^{-1}$) and k_{2r} ($2 \times 10^5 \text{ s}^{-1}$), respectively, because they reflect electron transfer rates between heme a_3 and heme a . Nonetheless, it is important to point out that the electron transfer rates between two redox centers might be affected by the redox states of the other two redox centers.

Fig. 7A shows the simulated result based on the rate constants listed above. The result shows that $\sim 60\%$ of the enzyme is in the c , c' , d , and d' states (with equal population). In addition, ~ 30 and 10% of the enzyme are in the b and e states, respectively. The dotted lines show the total amount of the redox species with either a reduced or an oxidized heme a_3 by summing up the contribution from each species. The data suggest that about 40% of the electron density in the photolyzed MVCO transfers out of heme a_3 . The failure to fit the kinetic data with the basis equilibrium spectra is attributed to the high population ($\sim 60\%$) of the c , c' , d , and d' species that consist only of one electron in the binuclear center.

Under equilibrium conditions, we assume that k_{2f} and k_{5r} are significantly reduced due to the protein structural transition from P_1 to P_2 that stabilizes the states with either zero (species e) or two (species b) electrons in the binuclear center with respect to those with only a single electron. Fig. 7B shows the simulation results based on this assumption by decreasing k_{2f} and k_{5r} by a factor of 10 and 70, respectively. All of the other rate constants are kept unchanged. With these two new rate constants, $\sim 60\%$ of the electron in the photolyzed MVCO transfers out of heme a_3 under the photostationary state conditions, which is consistent with the experimental results shown in Fig. 4. More importantly, under these conditions, the populations of species c , c' , d , and d' are negligible. As a result, the equilibrium data can be well fitted with the standard spectra.

A kinetic scheme that is similar to Scheme 2 has been proposed by Einarsdottir and co-workers (5, 6) based on optical absorption measurements following photodissociation of MVCO. In that work, spectral perturbations of the intermediate in both the Soret and visible regions of the optical absorption spectrum were observed in the microsecond time domain. The authors proposed that the redox state of Cu_B significantly affects the absorption spectrum of heme a_3 , similar to what we observed here in the resonance Raman spectra. They postulate

that there is a rapid equilibrium between reduced heme a_3 and reduced Cu_B when only one electron resides in the binuclear center, and this equilibrium favors the direction of reduced Cu_B because of its relatively higher E_m .

Modulation of electron redistribution following photolysis of MVCO by protein conformational changes has never been reported. However, conformational changes on faster time scales were documented by Einarsdottir *et al.* and Woodruff *et al.* (22, 31). In those studies, spectral changes in the visible region were observed on the picosecond time scale followed by additional changes on the microsecond time scale. The former is ascribed to be the conformational change triggered by the binding of CO to Cu_B , and the latter is suggested to be the relaxation of the conformational changes induced by the departure of CO from Cu_B , which occurs at about $1 \mu\text{s}$ (31). The picosecond time scale conformational change does not appear to disturb the Raman spectrum since the 10-ns spectrum is almost identical to the model spectrum B. It is plausible that the departure of the CO from Cu_B at $\sim 1 \mu\text{s}$ could leave the binuclear center in an unrelaxed metastable state that could affect the electron transfer rates. Furthermore, kinetic studies following the photodissociation of the CO-bound fully reduced enzyme demonstrate that the heme a_3 pocket undergoes significant reorganization upon photolysis, with the frequency of the Fe-His stretching mode evolving from 222 cm^{-1} at 10 ns to 214 cm^{-1} on a $\sim 10\text{-}\mu\text{s}$ time scale (33, 34). The conformational change we reported here in the mixed valence enzyme on the millisecond time scale could have a similar origin as that observed in these systems.

In summary, we have observed a modulation of the electron redistribution following photodissociation of CO from MVCO due to a conformational transition. Subsequent to photodissociation, the protein matrix is trapped transiently in the P_1 metastable state in which the initial electron transfer events occur within $5 \mu\text{s}$. It relaxes to the equilibrium P_2 conformation on a time scale longer than 2 ms. The conformational change destabilizes the redox states with a one-electron reduced binuclear center with respect to those that have either zero or two electrons. As a result, the redox equilibrium is perturbed, and electrons are redistributed. Under transient conditions when the protein matrix is in the P_1 conformation, $\sim 40\%$ of the electron density originally on heme a_3 is transferred to heme a . On the other hand, under equilibrium conditions when the protein matrix is in the P_2 conformation, $\sim 60\%$ of the electron density is transferred from heme a_3 to heme a . The conformational change-induced electron redistribution is confirmed by the simulation results with a new proposed kinetic model. Future work is planned to determine the molecular basis of the conformational change.

Acknowledgment—We thank Dr. Shinya Yoshikawa for advice on the preparation and purification of cytochrome *c* oxidase.

REFERENCES

- Babcock, G. T., and Wikstrom, M. (1992) *Nature* **356**, 301–309
- Ferguson-Miller, S., and Babcock, G. T. (1996) *Chem. Rev.* **96**, 2889–2908
- Malatesta, F., Antonini, G., Sarti, P., and Brunori, M. (1995) *Biophys. Chem.* **54**, 1–33
- Tsukihara, T., Aoyama, H., Yamashita, E., Tomizaki, T., Yamaguchi, H., Shinzawa-Itoh, K., Nakashima, R., Yaono, R., and Yoshikawa, S. (1995) *Science* **269**, 1069–1074
- Georgiadis, K. E., Jhon, N. I., and Einarsdottir, O. (1994) *Biochemistry* **33**, 9245–9256
- Einarsdottir, O., Georgiadis, K. E., and Sucheta, A. (1995) *Biochemistry* **34**, 496–508
- Oliveberg, M., and Malmstrom, B. G. (1991) *Biochemistry* **30**, 7053–7057
- Verkhovskiy, M. I., Morgan, J. E., and Wikstrom, M. (1992) *Biochemistry* **31**, 11860–11863
- Boelens, R., and Wever, R. (1979) *Biochim. Biophys. Acta* **547**, 296–310
- Boelens, R., Wever, R., and Van Gelder, B. F. (1982) *Biochim. Biophys. Acta* **682**, 264–272
- Brzezinski, P., and Malmstrom, B. G. (1987) *Biochim. Biophys. Acta* **894**, 29–38

12. Adelroth, P., Brzezinski, P., and Malmstrom, B. G. (1995) *Biochemistry* **34**, 2844–2849
13. Brzezinski, P. (1996) *Biochemistry* **35**, 5611–5615
14. Morgan, J. E., Verkhovsky, M. I., Puustinen, A., and Wikstrom, M. (1993) *Biochemistry* **32**, 11413–11418
15. Ching, E., Gennis, R. B., and Larsen, R. W. (2003) *Biophys. J.* **84**, 2728–2733
16. Verkhovsky, M. I., Jasaitis, A., and Wikstrom, M. (2001) *Biochim. Biophys. Acta* **1506**, 143–146
17. Namslauer, A., Branden, M., and Brzezinski, P. (2002) *Biochemistry* **41**, 10369–10374
18. Rousseau, D. L. (1981) *J. Raman Spectrosc.* **10**, 94–99
19. Yoshikawa, S., Choc, M. G., O'Toole, M. C., and Caughey, W. S. (1977) *J. Biol. Chem.* **252**, 5498–5508
20. Rousseau, D. L., and Han, S. (2002) *Methods Enzymol.* **354**, 351–368
21. Gibson, Q. H., and Greenwood, C. (1963) *Biochem. J.* **86**, 541–554
22. Einarsdottir, O., Dyer, R. B., Lemon, D. D., Killough, P. M., Hubig, S. M., Atherton, S. J., Lopez-Garriga, J. J., Palmer, G., and Woodruff, W. H. (1993) *Biochemistry* **32**, 12013–12024
23. Proshlyakov, D. A., Pressler, M. A., and Babcock, G. T. (1998) *Proc. Natl. Acad. Sci. U. S. A.* **95**, 8020–8025
24. Yoshikawa, S., Shinzawa-Itoh, K., and Tsukihara, T. (1998) *J. Bioenerg. Biomembr.* **30**, 7–14
25. Beinert, H., and Shaw, R. W. (1977) *Biochim. Biophys. Acta* **462**, 121–130
26. Shaw, R. W., Hansen, R. E., and Beinert, H. (1978) *J. Biol. Chem.* **253**, 6637–6640
27. Karlsson, B., and Andreasson, L. E. (1981) *Biochim. Biophys. Acta* **635**, 73–80
28. Reinhammar, B., Malkin, R., Jensen, P., Karlsson, B., Andreasson, L. E., Aasa, R., Vanngard, T., and Malmstrom, B. G. (1980) *J. Biol. Chem.* **255**, 5000–5003
29. Jensen, P., Aasa, R., and Malmstrom, B. G. (1981) *FEBS Lett.* **125**, 161–164
30. Witt, S. N., Blair, D. F., and Chan, S. I. (1986) *J. Biol. Chem.* **261**, 8104–8107
31. Woodruff, W. H., Einarsdottir, O., Dyer, R. B., Bagley, K. A., Palmer, G., Atherton, S. J., Goldbeck, R. A., Dawes, T. D., and Kliger, D. S. (1991) *Proc. Natl. Acad. Sci. U. S. A.* **88**, 2588–2592
32. Morgan, J. E., Li, P. M., Jang, D. J., el-Sayed, M. A., and Chan, S. I. (1989) *Biochemistry* **28**, 6975–6983
33. Findsen, E. W., Centeno, J. A., Babcock, G. T., and Ondrias, M. R. (1987) *J. Am. Chem. Soc.* **109**, 5367–5372
34. Lou, B.-S., Larsen, R. W., Chan, S. I., and Ondrias, M. R. (1993) *J. Am. Chem. Soc.* **115**, 403–407